2024 NDIA MICHIGAN CHAPTER
GROUND VEHICLE SYSTEMS ENGINEERING
AND TECHNOLOGY SYMPOSIUM
POWER & MOBILITY TECHNICAL SESSION
AUGUST 13-15, 2024 - NOVI, MICHIGAN

DEFECT-RICH REDUCED GRAPHITIC CARBON NITRIDE AS THE SULFUR HOST MATERIAL FOR LITHIUM-SULFUR BATTERIES

Aliakbar Yazdani[1], Jyoti Pandey[2], Mukesh Jakhar[2], Benjamin R. Seltin[1], Veronica Barone[2], Valeri Petkov[2], Yi Ding[3], Bradley D. Fahlman[1]

[1] Department of Chemistry & Biochemistry, Central Michigan University, Mount Pleasant, MI
[2] Department of Physics, Central Michigan University, Mount Pleasant, MI
[3] U.S. Army Ground Vehicle Systems Center, 6305 E. 11th Mile Rd., Warren, MI 48092

ABSTRACT

Defect-rich reduced graphitic carbon nitride was synthesized using a facile and scalable technique and utilized as the host material for sulfur as the active cathode material for lithium-sulfur batteries. Multiple analytical and electrochemical tests were conducted to understand and optimize the physiochemical properties of the reduced graphitic carbon nitride for battery application. By utilizing this sulfur host, the specific capacity of the battery increased by up to 2X over pristine graphitic carbon nitride host at lower charge/discharge rates. The presence of defects and higher porosity compared to pristine graphitic carbon nitride were shown to be the main difference between these sulfur hosts.

Citation: A. Yazdani, J. Pandey, M. Jakhar, B. Seltin, V. Barone, V. Petkov, Y. Ding, B. D. Fahlman, "Defect-Rich Reduced Graphitic Carbon Nitride as the Sulfur Host Material for Lithium-Sulfur Batteries," In *Proceedings of the Ground Vehicle Systems Engineering and Technology Symposium* (GVSETS), NDIA, Novi, MI, Aug. 13-15, 2024.

1. INTRODUCTION

The pursuit of high-energy-density energy storage systems has steered extensive research toward lithium-sulfur (Li-S) batteries [1]. While demonstrating theoretical potential, Li-S batteries grapple with significant challenges, notably, capacity fading due to inefficient redox reactions, the shuttle effect causing polysulfide dissolution, and sluggish reaction kinetics. Capacity retention, or the ability to maintain a consistent energy storage capacity over multiple charge-discharge cycles, is one of the foremost challenges plaguing Li-S batteries [1]. This issue stems from the dissolution of intermediate polysulfides during cycling, resulting in reduced active sulfur species and decreased overall battery capacity. The shuttle effect exacerbates capacity fading by causing the diffusion of polysulfide species across the electrolyte, leading to active material loss, reduced coulombic efficiency, and premature

degradation [2], [3]. Furthermore, the sluggish redox reactions between sulfur and lithium ions impede the overall battery kinetics, resulting in poor rate capability and limited power output [4]. This sluggishness hampers the ability of the battery to deliver and accept charge rapidly, especially during high current demands. To address these challenges, recent research has shown promising avenues in the utilization of graphitic carbon nitride (g-C_3N_4) in Li-S batteries. Graphitic carbon nitride demonstrates the ability to confine polysulfides, enhance sulfur utilization, and improve overall battery performance [5]. Its high surface area and chemical stability make it an ideal candidate to trap polysulfides and alleviate the shuttle effect, thereby contributing to enhanced capacity retention and reaction kinetics in Li-S batteries. The incorporation of defects in graphitic carbon nitride (g-C_3N_4) has been demonstrated to significantly enhance its catalytic performance in various energy storage and conversion applications. Compared to pristine graphitic carbon nitride (pg-C_3N_4), defect-rich reduced (rg-C_3N_4) analogs exhibit superior electrocatalytic activity. This may be attributed to the presence of nitrogen vacancies and edge sites, which serve as active sites for catalyzing sulfur redox reactions and adsorbing polysulfides [6]. These defects facilitate efficient charge transfer and promote the formation of stable intermediates, thereby improving the kinetics of sulfur conversion and mitigating polysulfide shuttling in metal-sulfur batteries [7]. Additionally, rg-C_3N_4 offers enhanced chemical and thermal stability, leading to prolonged cycling stability and improved overall performance of metal-sulfur batteries [8]. Furthermore, the introduction of defects in g-C_3N_4 enables tailored band structure engineering, which further enhances its catalytic activity and enables precise control over the electrochemical behavior of metal-sulfur battery systems [9]. In this article, we describe two different ways of introducing defects to pristine g-C_3N_4 and their effect on the electrochemical performance of cathodes in lithium-sulfur cells.

2. EXPERIMENTAL

The cathode of the lithium-sulfur battery was the focus of this study. To produce and test the performance of the cathode materials the following steps were conducted.

2.1. Material Synthesis

Pristine graphitic carbon nitride (pg-C_3N_4) was synthesized from pure urea in an alumina crucible covered with a lid was heated at 550 °C for 4 h at a heating rate of 2.5 °C.min^{-1} in a muffle furnace. A yellow-colored powder was obtained, which was used further for incorporating defects into the graphitic matrix of carbon nitride. For this, two different approaches were adopted, i.e., magnesiothermal and thermal treatment *in vacuo*.

Synthesis of reduced g-C_3N_4 via magnesiothermal (MT-rg-C_3N_4) method: Pristine g-C_3N_4 was mixed with magnesium powder (2:1 (w/w)) and placed in a stainless-steel crucible with a lid and heated to 750 °C for 2 h in a tube furnace under a flow of ultra-high purity (UHP) argon. The obtained reduced graphitic carbon nitride was washed several times with dilute acetic acid and distilled water to remove metal impurities and byproducts, followed by vacuum drying.

Synthesis of reduced g-C_3N_4 via thermal treatment *in vacuo*: The synthesized pristine g-C_3N_4 was placed in a tube furnace under vacuum to prevent exposure to oxygen during heating steps. The sample was then heated to 590 °C for 4 h at a heating rate of 2.5 °C.min^{-1} and then cooled down under vacuum before removing from the furnace.

Synthesis of carbon nitride and sulfur composites (C-S composite): The composites of carbon nitride and sulfur were prepared

using the melt infusion method. Pristine g-C_3N_4 was infused with sulfur, resulting in 60 wt% of sulfur in the final composite. In comparison, both reduced g-C_3N_4 samples contained 75 wt% of sulfur due to the additional pore volume of the carbon nitride host material. The samples were transferred into a Teflon-lined hydrothermal reactor and heated at 155 °C for 12 h to infiltrate the sulfur into the mesopores of the host materials.

2.2. Analytical Tests

X-ray diffraction (XRD) was employed to study the phase transitions and crystal structures of the samples. All X-ray data was obtained using a Rigaku MiniFlex II with monochromatic Cu K∝ radiation of 1.54 Å. Samples were scanned from 2Θ values of 10° to 80° at a scan rate of 0.5 degrees/min. Thermogravimetric analysis (TGA) of the carbon hosts (g-C_3N_4 and rg-C_3N_4) and C-S composites (g-C_3N_4-S and rg-C_3N_4-S) was carried out using a simultaneous TGA/DSC instrument (SDT Q600, TA instruments). To carry out the analyses, ca. 5 mg of each sample was placed in a ceramic pan to determine the decomposition temperature and mass loss. The sample was heated from room temperature to 600 °C at a heating rate of 10 °C/min in an ultra-high purity N_2 environment flowing at 20 mL/min. The Brunauer−Emmett−Teller (BET) method was used for surface area calculations whereas Barrett− Joyner−Halenda (BJH) methods were used for the pore sizes and pore volume calculations. The degassing profiles for g-C_3N_4 samples were 180 °C for 3 hours. Raman spectroscopy was carried out with a Horiba Xplora One spectrometer equipped with a 532 nm laser and a 100×objective. X-ray photoelectron spectroscopy (XPS, Kratos Axis Ultra) was utilized to study the extent of defect generation during the reduction step of g-C_3N_4.

2.3. Electrochemical Study

All electrolyte solutions were prepared in an argon-filled glovebox with O_2 and H_2O concentrations less than 0.1 ppm. To prepare the electrolyte, 2.87 g of lithium bis(trifluoromethane)sulfonimide (LiTFSI) was dissolved in 10 mL of an ether-based solvent mixture of dimethoxyethane and 1,3-dioxolane (DME-DOL, 1:1); 1% wt. of lithium nitrate ($LiNO_3$) was also dissolved in the electrolyte as an additive to protect the anode. The electrolyte solution was stirred overnight to ensure all particles were dissolved. The electrodes were fabricated via slurry casting using a doctor blade, the cathode slurry consisted of the active material (C-S composite), carbon black, and polyvinylidene fluoride binder, in a weight ratio of 7:2:1, dissolved in N-methyl-2-pyrrolidone (NMP) solvent. The slurry mixture was transferred into a 20 mL zirconia (ZrO_2) grinding bowl along with 30 ZrO_2 balls and ball-milled at 1100 RPM for 1 h to achieve a homogenous mixture. The homogenous slurry was then coated on an aluminum current collector using a doctor blade. The coated aluminum foil was vacuum dried overnight at 60 °C, then punched into a circular disc of 16 mm diameter and weighed to determine the active mass and areal loading. The punched discs were then transferred into the glovebox for final coin cell fabrication. The fabricated coin-cells consisted of the punched cathode disc, lithium disc as the anode (reference electrode), microporous polypropylene separator (Celgard, USA), and 1 M LiTFSI with 1% wt. $LiNO_3$ dissolved in DOL:DME as the electrolyte.

The fabricated CR2032 type coin cells were galvanostatically cycled (charged-discharged) at various current densities (C-rate) within the voltage window 1.7-2.8 V vs. Li/Li^+. The galvanostatic charge and discharge cycling was carried out using an automatic battery testing system, Maccor

series 4600A. The specific capacities were calculated based on the mass of active sulfur in the cathode. Charge/discharge rates are described based on C-rates (where 1C = 1672 $mAhg^{-1}$, the theoretical capacity for the complete electrochemical reduction of S to Li_2S).

3. Result and Discussion

3.1. Analytical Tests

The graphitization of carbon nitride was confirmed by the XRD studies (Figure 1). The XRD patterns of bulk-g-C_3N_4 and reduced-g-C_3N_4 have a strong peak of (002) around 2θ =27.5° and a weak peak of (100) at about 12.9° [10]. The (002) crystal plane with a strong diffraction peak was attributed to the layer stacking of aromatic systems. The (100) crystal plane was related to the in-planar repeating triazine unit. The weaker intensity peaks of the rg-C_3N_4 sample are suggestive of a decrease in the order of filling of the in-plane structure due to more structural defects and decreased thickness of rg-C_3N_4 caused by pressure-thermal dual driving forces during the preparation process [11].

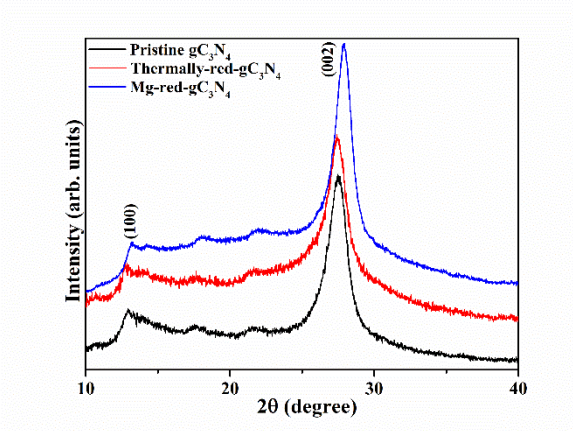

Figure 1. XRD analysis of pristine, thermally reduced, and magnesiothermally reduced g-C_3N_4

TGA analysis (under O_2) was performed on both pristine and thermally reduced g-C_3N_4 which showed a lower decomposition temperature for the reduced sample. The presence of defects resulted in more reactivity with oxygen at lower temperatures (Figure 2)

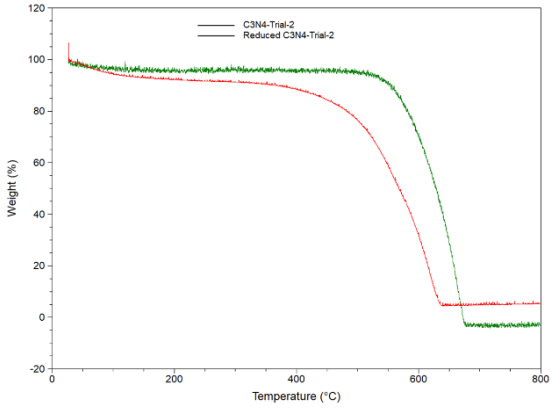

Figure 2. TGA analysis of pristine and thermally reduced g-C_3N_4

X-ray photoelectron spectroscopy (XPS) showed the presence of C-O bonds indicating partial oxygenation of rg-C_3N_4. C-C peaks in the rg-C_3N_4 sample shows the removal of some N from the structure of C_3N_4 (Figure 3)

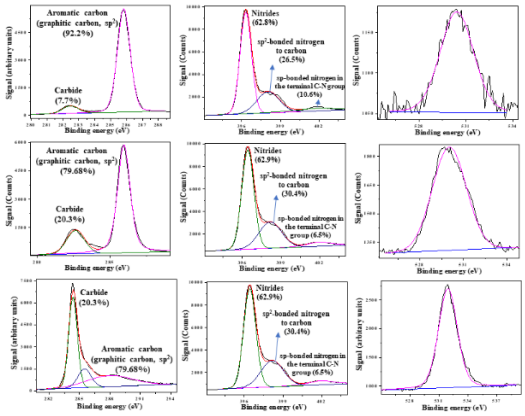

Figure 3. XPS data for thermally reduced g-C_3N_4

The porosity and microstructure of the samples were characterized with nitrogen adsorption-desorption measurements at 77 K providing detailed information about the specific surface area and pore distribution.

The sorption isotherms exhibit the IUPAC type-IV isotherm characterized by the hysteresis loop at P/P_o = 0.4-1.0 which indicates the presence of both micro and mesopores. The pore volume along with the BET surface area for pristine and reduced g-C_3N_4 is presented in Table 2. The results indicate the introduction of nitrogen defects upon reducing the pristine sample, which led to increased surface areas. Further, this can serve as an effective conduit for ion mobility and better electrolyte-electrode interface interactions.

Table 1. BET surface area and pore volume of pristine, thermally reduced, and magnesiothermally reduced g-C_3N_4

Sample	BET surface area (m^2/g)	Pore Volume (cc/g)
pg-C_3N_4	121	0.027
Thermally reduced g-C_3N_4	188	0.182
Magnesiothermal reduced g-C_3N_4	171	0.049

Nanocrystalline graphitic carbon based materials are often characterized by two major Raman bands related to the graphitic carbon (G) and the disordered carbon (D) [12]. The prominent peaks located at ~1330 and 1580 cm^{-1} indicate the D and G bands of g-C_3N_4, respectively. It is known that the intensity ratio of the two peaks (i.e., I_D/I_G) can be correlated to the size of the sp^2 C cluster in the material. Since the I_D/I_G ratio is directly proportional to the defect density in the system, the higher ratio indicates the development of defect sites in the network (Figure 4) [13].

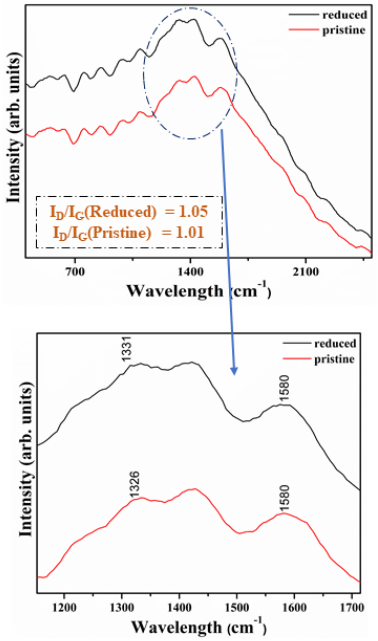

Figure 4. Raman spectroscopy data for pristine and thermally reduced g-C_3N_4

To test the electrochemical performance of the pristine graphitic carbon nitride thermally reduced graphitic carbon nitride and magnesiothermal reduced graphitic carbon nitride as the sulfur host, coin cells were assembled with cathode made as described in the experimental section, and galvanostatically cycled with pure lithium metal anode in the voltage window of 1.7-2.8 V. Figure 5 presents the electrochemical performance of lithum sulfur cells at various C-rates. C-S composites as cathode material showed a very high initial discharge of around 1600 mAh/g that rapidly faded to about 400 mAh/g. Capacity fading, a common phenomenon in Li-S cells, could be attributed to the polysulfide shuttle effect and the poor conductivity of the carbon host, which results in very slow kinetics and precipitation of the non-conductive layer of Li_2S at the surface of the cathode. The pristine gCN-S cathode exhibits lower capacities compared to both thermally

reduced and magensiothermally reduced g-C_3N_4.

Of the two reduced g-C_3N_4 samples, the magnesiothermal sample resulted in slightly higher capacity compared to the thermally reduced sample even though XRD showed less structural disorder. The higher degree of surface area and pore volume resulting from the higher synthesis temperature was likely responsible for the performance improvement of this sample.

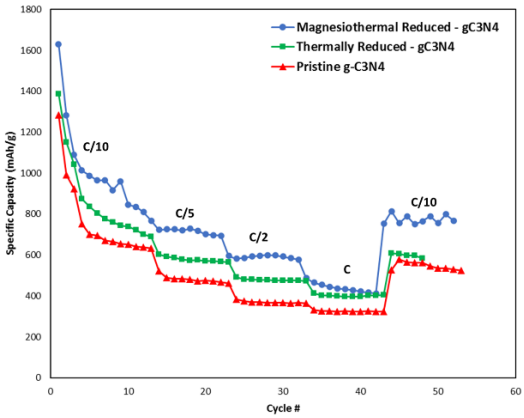

Figure 5. Discharge specific capacity of lithium-sulfur cells made using pristine, thermally reduced, and magnesiothermally reduced g-C_3N_4 as the sulfur host.

3.2. Theoretical calculations

Spin-polarized density functional theory (DFT) calculations were performed using the Vienna Ab-initio Simulation Package (VASP) [14]. The exchange correlation energy was described using the gradient corrected Perdew–Burke–Ernzerhof (GGA-PBE) functional and the projector augmented wave (PAW) method [15]. In addition, Van der Waals interactions were included utilizing the Grimme DFT-D3 correction scheme [16]. For the plane-wave expansion, the cutoff energy was set to 520 eV. During the geometric optimization of polysulfides adsorbed on the substrates, relaxation of atomic positions was carried out with a constant cell shape until the residual force reached a threshold of less than 0.01 eV/Å. A 20 Å vacuum space along the *z*-direction was considered to prevent interactions with adjacent periodic images.

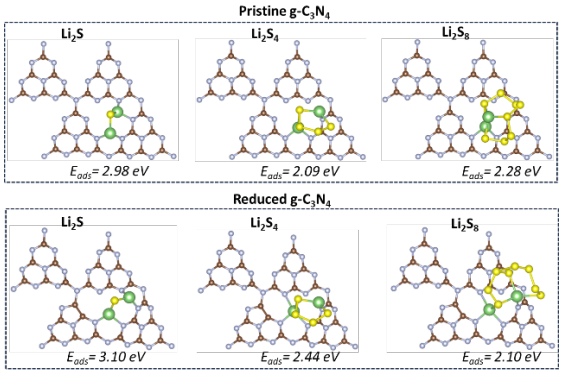

Figure 6. The optimized geometric configurations of Li_2S_x (x=1, 4, 8) on the pristine and reduced g-C_3N_4 surface.

As shown in Figure 6, the adsorption energy was computed to gauge the strength between substrates (pristine and reduced g-C_3N_4) and the polysulfides. The adsorption energy is defined as:

$$E_{ads} = E_{Poly} + E_{Sub} - E_{Poly\_Sub}$$

where E_{Poly_Sub}, E_{Poly}, and E_{Sub} are the energies of the polysulfides+substrate, polysulfides, and substrate, respectively. According to this definition, a positive E_{ads} indicates a stronger anchoring effect of polysulfides on the substrate. Our calculations indicate that the adsorption of Li_2S_x (x=1, 4, 8) on pristine (reduced) g-C_3N_4 are 2.98 (3.10) eV, 2.09 (2.44) eV, and 2.28 (2.10) eV, respectively. The strongest adsorption appears in the stage of Li_2S on pristine g-C_3N_4 (Fig. 6). Following reduction (N-deficient), the corresponding adsorption energies are 3.10 eV on the reduced g-C_3N_4 surface, respectively, even higher than those on the pristine g-C_3N_4. Thus, the reduced g-C_3N_4 shows a superior ability to adsorb Li_2S than pristine g-C_3N_4.

4. REFERENCES

[1] A. Manthiram, Y. Fu, and Y.-S. Su, "Challenges and Prospects of Lithium–Sulfur Batteries," *Acc. Chem. Res.*, vol. 46, no. 5, pp. 1125–1134, May 2013, doi: 10.1021/ar300179v.

[2] J. Zhang, W. Cai, F. Xin Hu, H. Yang, and B. Liu, "Recent advances in single atom catalysts for the electrochemical carbon dioxide reduction reaction," *Chemical Science*, vol. 12, no. 20, pp. 6800–6819, 2021, doi: 10.1039/D1SC01375K.

[3] L. Zou, Y.-S. Wei, C.-C. Hou, C. Li, and Q. Xu, "Single-Atom Catalysts Derived from Metal–Organic Frameworks for Electrochemical Applications," *Small*, vol. 17, no. 16, p. 2004809, 2021, doi: 10.1002/smll.202004809.

[4] Z. Liang *et al.*, "Advances in the Development of Single-Atom Catalysts for High-Energy-Density Lithium–Sulfur Batteries," *Advanced Materials*, vol. 34, no. 30, p. 2200102, 2022, doi: 10.1002/adma.202200102.

[5] J. Chen *et al.*, "Nitrogen-Deficient Graphitic Carbon Nitride with Enhanced Performance for Lithium Ion Battery Anodes," *ACS Nano*, vol. 11, no. 12, pp. 12650–12657, Dec. 2017, doi: 10.1021/acsnano.7b07116.

[6] H. Liu *et al.*, "Defective engineering in graphitic carbon nitride nanosheet for efficient photocatalytic pathogenic bacteria disinfection," *Applied Catalysis B: Environmental*, vol. 261, p. 118201, Feb. 2020, doi: 10.1016/j.apcatb.2019.118201.

[7] H. Xu, L. Ma, and Z. Jin, "Nitrogen-doped graphene: Synthesis, characterizations and energy applications," *Journal of Energy Chemistry*, vol. 27, no. 1, pp. 146–160, Jan. 2018, doi: 10.1016/j.jechem.2017.12.006.

[8] H. Ma *et al.*, "Defect-rich porous tubular graphitic carbon nitride with strong adsorption towards lithium polysulfides for high-performance lithium-sulfur batteries," *Journal of Materials Science & Technology*, vol. 115, pp. 140–147, Jul. 2022, doi: 10.1016/j.jmst.2021.10.044.

[9] S. Yao *et al.*, "Synthesis of graphitic carbon nitride at different thermal-pyrolysis temperature of urea and it application in lithium–sulfur batteries," *J Mater Sci: Mater Electron*, vol. 29, no. 20, pp. 17921–17930, Oct. 2018, doi: 10.1007/s10854-018-9906-2.

[10] T. Liu *et al.*, "Preparation of Structure Vacancy Defect Modified Diatomic-Layered g-C3N4 Nanosheet with Enhanced Photocatalytic Performance," *Advanced Science*, vol. 10, no. 24, p. 2302503, 2023, doi: 10.1002/advs.202302503.

[11] J. Cao, W. Nie, L. Huang, Y. Ding, K. Lv, and H. Tang, "Photocatalytic activation of sulfite by nitrogen vacancy modified graphitic carbon nitride for efficient degradation of carbamazepine," *Applied Catalysis B: Environmental*, vol. 241, pp. 18–27, Feb. 2019, doi: 10.1016/j.apcatb.2018.09.007.

[12] S. Bayan, A. Midya, N. Gogurla, A. Singha, and S. K. Ray, "Origin of Modified Luminescence Response in Reduced Graphitic Carbon Nitride Nanosheets," *J. Phys. Chem. C*, vol. 121, no. 35, pp. 19383–19391, Sep. 2017, doi: 10.1021/acs.jpcc.7b06587.

[13] J. Jiang *et al.*, "Dependence of electronic structure of g-C3N4 on the layer number of its nanosheets: A study by Raman spectroscopy coupled with first-principles calculations," *Carbon*, vol. 80, pp. 213–221, Dec. 2014, doi: 10.1016/j.carbon.2014.08.059.

[14] G. Kresse *et al*., " Efficient iterative schemes for ab initio total-energy

calculations using a plane-wave basis set" *Physical review B*, vol. 54, pp. 11169, Oct. 1996, doi: 10.1103/PhysRevB.54.11169.

[15] J. P. Perdew *et al*., " Generalized Gradient Approximation Made Simple" *Physical review letters,* vol. 77, pp. 3865, May. 1996, doi: 10.1103/PhysRevLett.77.3865.

[16] S. Grimme *et al*., " A consistent and accurate ab initio parametrization of density functional dispersion correction (DFT-D) for the 94 elements H-Pu" *J. Chem. Phys.* vol. 132, pp. 154104, Mar. 2010, doi: 10.1063/1.3382344.